Near-infrared benzodiazoles as small molecule environmentally-sensitive fluorophores

Near-infrared benzodiazoles as small molecule environmentally-sensitive fluorophores

Fabio de Moliner,[1] Ina Biazruchka,[2] Karolina Konsewicz,[1] Sam Benson,[1] Suraj Singh,[1] Jun-Seok Lee,[3,*] Marc Vendrell,[1,*]

[1] Centre for Inflammation Research, Queen's Medical Research Institute, The University of Edinburgh, Edinburgh, UK.

[2] Molecular Recognition Research Centre, Korea Institute of Science and Technology (KIST) & Bio-Med Program, KIST-School UST, Seoul, 02792, South Korea.

[3] Department of Pharmacology, Korea University College of Medicine, Seoul, 02841, South Korea.

Abstract

The development of fluorophores emitting in the near-infrared spectral window has gained increased attention given their suitable features for biological imaging. In this work, we have optimised a general and straightforward synthetic approach to prepare a small library of near-infrared-emitting C-bridged nitrobenzodiazoles using commercial precursors. C-bridged benzodiazoles have low molecular weight and neutral character as important features that are not common in most near-infrared dyes. We have investigated their fluorescence response in the presence of a wide array of 60 different biomolecules and identified compound **3i** as a potential chemosensor to discriminate between Fe^{2+} and Fe^{3+} ions in aqueous media.

Introduction

The development of chemical structures showing enhanced fluorescence emission upon recognition of molecular analytes is an active area of research in analytical chemistry and molecular imaging [1-5]. In addition to their utility as highly sensitive analytical probes for environmental (e.g., metal ion detection) or biological measurements (e.g., quantification of biomarkers in clinical samples) [6-11], they have been increasingly used to derivatise bioactive molecules (e.g., peptides, proteins, antibodies) and to prepare complex molecular constructs [12-17]. The resulting architectures combine good selectivity for receptors and/or cells of interest as well as high sensitivity derived from environmentally- sensitive readouts, and have been reported as useful tools for *in vivo* imaging of specific biological processes or subpopulations of cells [18-24]. Among the different chemical structures employed for the development of fluorescent probes, those with emission wavelengths in the NIR (near-infrared) range (i.e., 650-900 nm) have received considerable attention [25-29]. NIR fluorophores benefit from the inherently low autofluorescence of biomolecules and tissues in a biological 'silent' window as well as the minimal toxicity derived from light irradiation at relatively long excitation wavelengths.

Our groups and many others have contributed to the synthesis and characterisation of NIR fluorescent structures with very diverse chemical scaffolds (Figure 1). Some of the most used include Si-rhodamines [30, 31], phthalocyanines [32-34], squaraines [35, 36], porphyrins [37], tricarbocyanines [38, 39], and the recently reported flavylium polymethines with emission wavelengths over 1000 nm [40]. One common feature of all these NIR-emitting scaffolds is their relatively large hydrophobicity, which can result in limited water solubility (e.g., charged groups such as sulfonates are often needed to enhance solubility in aqueous media) as well as their large molecular size, which can hamper the retention of bioactivity when derivatising peptides and proteins. C-bridged nitrobenzodiazoles have been recently described as chemical structures with relatively small size (<300 Da) and neutral character [41]. These properties can facilitate their application for labelling metabolites (e.g., lipids, sugars) as well as their translation to NIR bioimaging. However, with only a couple of examples being reported to date, the systematic evaluation of the C-bridged nitrobenzodiazole scaffold for the development of turn-on molecular probes has not been addressed.

Diversity-oriented fluorescent libraries have been described as a powerful approach for the discovery of new chemosensors [42]. Pioneered by Chang and co-workers, many turn-on fluorescent probes have been identified through the combinatorial derivatisation of fluorophore scaffolds and their systematic screening against biologically-relevant analytes [43-45]. One important advantage of this approach is its versatility, making it compatible with a broad range of chemical structures (including NIR fluorophores) and many different biological analytes. In the present work, we describe a synthetic methodology for the preparation of a small yet diverse collection of C-bridged nitrobenzodiazoles and their systematic spectral characterisation against multiple biomolecules, including sugars, lipids, amino acids and metal ions, among others. Through an *in vitro* fluorescence screening, we identified the benzodiazole **3i** as a fluorophore for recognition of Fe^{2+} ions. Our results demonstrate the potential utility of the C-bridged nitrobenzodiazole scaffold for the preparation of NIR-emitting activatable probes of smaller size than conventional NIR fluorophores.

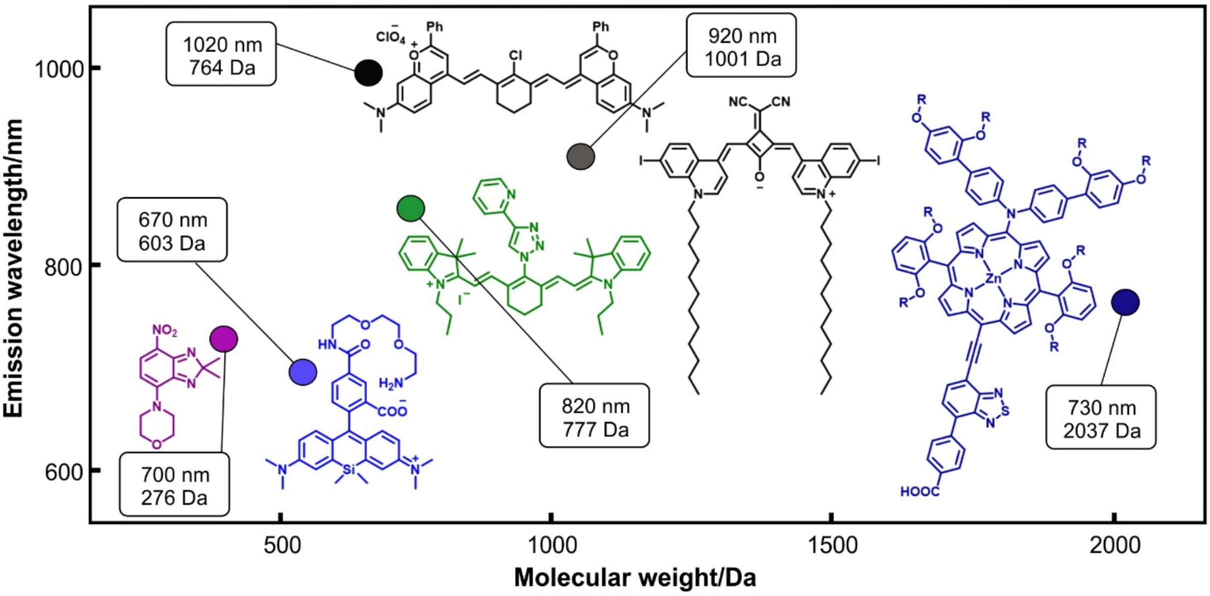

Figure 1. Structures and featured properties of NIR fluorophores that are representative of different chemical scaffolds.

Experimental

General materials. Commercially available reagents were used without further purification. Bioanalytes for the screening were obtained from Sigma-Aldrich, TCI and Junsei Chemical. Thin-layer chromatography was conducted on Merck silica gel 60 F254 sheets and visualized by UV (254 and 365 nm). Silica gel (particle size 35–70 μm) was used for column chromatography. ^{1}H and ^{13}C spectra were recorded in a Bruker Avance 500 spectrometer (at 500 and 125 MHz, respectively). Data for ^{1}H NMR spectra are reported as chemical shift δ (ppm), multiplicity, coupling constant (Hz) and integration. Data for ^{13}C NMR spectra reported as chemical shifts relative to the solvent peak. HPLC-MS analysis was performed on a Waters Alliance 2695 separation module connected to a Waters PDA2996 photodiode array detector and a ZQ Micromass mass spectrometer (ESI-MS) with a Phenomenex® column (C_{18}, 5 μm, 4.6 × 150 mm). High-resolution mass spectra (HRMS) were acquired using LTQ Orbitrap Velos with resolving power >100,000. High-throughput *in vitro* screening was performed on a FlexStation3 Multi-Mode Microplate Reader.

Synthesis of 3-fluoro-6-nitrobenzene-1,2-diamine (1). 3-Fluoro-6-nitrobenzoselenadiazole (2.9 mmol) were dissolved in HCl_{conc} (30 mL) and HI 57% (7.5 mL) was added dropwise. The reaction was stirred for 1 h at r.t. and then a saturated aqueous solution of Na_2SO_3 (100 mL) was added. Afterwards, an aqueous solution of 2 N NaOH was added dropwise until the pH reached 8. The solution was filtered through Celite and extracted with EtOAc (4 × 100 mL). The organic phase was dried over anhydrous $MgSO_4$ and the solvent was removed under reduced pressure to render a dark red solid. Crude product were purified by column chromatography (Hexane:EtOAc, 7:3) to give compound **1** as an orange solid (130 mg, 85% yield).

^{1}H NMR (500 MHz, DMSO-d_6) δ 7.40 (dd, J = 9.6, 5.8 Hz, 1H), 7.14 (s, 2H), 6.52 (t, J = 9.7 Hz, 1H), 5.15 (s, 2H).

^{13}C NMR (125 MHz, DMSO-d_6) δ 152.6 (d, $J_{C\text{-}F}$ = 242.0 Hz), 137.8 (d, $J_{C\text{-}F}$ = 9.9 Hz), 128.6, 124.3 (d, $J_{C\text{-}F}$ = 16.1 Hz), 114.2 (d, $J_{C\text{-}F}$ = 10.1 Hz), 104.8 (d, $J_{C\text{-}F}$ = 23.2 Hz).

HRMS (m/z, ESI): calcd for $C_6H_7FN_3O_2^+$ [M+H]$^+$: 172.0444, found: 172.0442.

General procedure A for the synthesis of 2-fluorobenzazoles (2a-2c). To a solution of compound **1** (1 eq) in EtOH (5 mL), $Cu(OAc)_2$ (0.05 eq) was added, followed by the corresponding ketone (10 eq). Reaction was heated at 80ºC overnight. Then, the reaction mixture was filtered through Celite and the solvent was removed under reduced pressure to give the crude products, which were purified by column chromatography.

Synthesis of compound 2a. Prepared according to general procedure A. Crude product was purified by column chromatography (DCM:Hexane, 1:1) to give compound **2a** as a red solid (10 mg, 80% yield).

Synthesis of compound 2b. Prepared according to general procedure A. Crude product was purified by column chromatography (Hexane:EtOAc, 8:2) to give compound **2b** as a red solid (3 mg, 6% yield).

Synthesis of compound 2c. Prepared according to general procedure A. Crude product was purified by column chromatography (DCM:Hexane, 7:3) to give compound **2c** as a red solid (20 mg, 37% yield).

General procedure B for the synthesis of 2-aminobenzazoles (3a-3k). To solutions of compounds **2a-2c** (1 eq) in MeCN (1 mL), $NaHCO_3$ (2.5 eq) in H_2O (1 mL) was added, followed by amines (1 eq) and the reactions were heated at 65ºC or stirred at r.t. until completion. The reaction mixtures were diluted with EtOAc and washed with 0.2 N HCl and brine. Organic layers were dried over anhydrous $MgSO_4$, concentrated under reduced pressure and purified by column chromatography or preparative TLC.

Synthesis of compound 3a. Prepared from **2a** according to general procedure B upon heating at 65 ºC for 3 h. Crude product was purified by column chromatography (DCM:MeOH, 95:5) to give compound **3a** as a purple solid (2 mg, 80% yield).

Synthesis of compound 3b. Prepared from **2b** according to general procedure B upon heating at 65 °C for 40 min. Crude product was purified by column chromatography (DCM:EtOAc, 9:1) to give compound **3b** as a purple solid (1 mg, 60% yield).

Synthesis of compound 3c. Prepared from **2c** according to general procedure B upon heating at 65 °C for 1 h. Crude product was purified by column chromatography (Hexane:EtOAc, 4:6) to give compound **3c** as a purple solid (1 mg, 9% yield).

Synthesis of compound 3d. Prepared from **2a** according to general procedure B upon stirring overnight at r.t. Crude product was purified by preparative TLC (DCM:MeOH, 95:5) to give compound **3d** as a purple solid (2 mg, 23% yield).

Synthesis of compound 3e. Prepared from **2a** according to general procedure B upon stirring overnight at r.t. Crude product was purified by preparative TLC (DCM:MeOH, 95:5) to give compound **3e** as a purple solid (2 mg, 40% yield).

Synthesis of compound 3f. Prepared from **2a** according to general procedure B upon heating at 65 °C for 2 h. Crude product was purified by column chromatography (DCM:MeOH, 95:5) to give compound **3f** as a purple solid (5 mg, 41% yield).

Synthesis of compound 3g. Prepared from **2a** according to general procedure B upon stirring overnight at r.t. Crude product was purified by preparative TLC (DCM:MeOH, 95:5) to give compound **3g** as a purple solid (3 mg, 34% yield).

Synthesis of compound 3h. Prepared from **2a** according to general procedure B upon stirring overnight at r.t. Crude product was purified by column chromatography (DCM:MeOH, 95:5) to give compound **3h** as a purple solid (1 mg, 4% yield).

Synthesis of compound 3i. Prepared from **2a** according to general procedure B upon stirring overnight at r.t. Crude product was purified by preparative TLC (DCM:MeOH, 95:5) to give compound **3i** as a purple solid (1 mg, 15% yield).

Synthesis of compound 3j. Prepared from **2a** according to general procedure B heating at 65 °C for 1 h. Crude product was purified by preparative TLC (DCM:MeOH, 95:5) to give compound **3j** as a purple solid (2 mg, 24% yield).

Synthesis of compound 3k. Prepared from **2a** according to general procedure B upon stirring overnight at r.t. Crude product was purified by preparative TLC (DCM:MeOH, 95:5) to give compound **3k** as a brown solid (1 mg, 7% yield).

Scale-up synthesis of compound 2a. To a solution of compound **1** (0.3 mmol, 51 mg, 1 eq) in EtOH (5 mL), $Cu(OAc)_2$ (0.015 mmol, 3 mg, 0.05 eq) was added, followed by acetone (30 mmol, 2.2 mL, 10 eq). Reaction was heated at 80ºC overnight. Then, the reaction mixture was filtered through Celite and the solvent was removed under reduced pressure to give the crude product, that was purified by column chromatography (DCM:Hexane, 1:1) to give compound **2a** as a red solid (44 mg, 70% yield).

^{1}H NMR (500 MHz, CD_2Cl_2) 7.19 (dd, J = 9.6, 4.6 Hz, 1H), 6.26 (dd, J = 9.3, 8.4 Hz, 1H), 1.52 (s, 6H).

^{13}C NMR (125 MHz, CD_2Cl_2) δ 149.2 (d, $J_{C\text{-}F}$ = 243.8 Hz), 141.5 (d, $J_{C\text{-}F}$ = 11.2 Hz), 126.7 (d, $J_{C\text{-}F}$ = 17.1 Hz), 114.9 (d, $J_{C\text{-}F}$ = 8.5 Hz), 107.1 (d, $J_{C\text{-}F}$ = 22.2 Hz), 81.9, 30.2.

HRMS (m/z, ESI): calcd for $C_9H_9FN_3O_2^+$ [M+H]$^+$: 210.0673, found: 210.0673.

Scale-up synthesis of hit compound 3i. To a solution of compound **2a** (0.09 mmol, 19 mg, 1 eq) in MeCN (1 mL), $NaHCO_3$ (0.23 mmol, 20 mg, 2.5 eq) in H_2O (1 mL) was added, followed by morpholine (0.23 mmol, 18 μL, 2.5 eq) and the reaction was stirred at r.t. for 28 h. The reaction mixture was diluted with EtOAc and washed with 0.2 N HCl and brine. Organic layer was dried over anhydrous $MgSO_4$, concentrated under reduced pressure and purified by column chromatography (DCM:MeOH, 95:5) to give **3i** as a purple solid (3 mg, 13% yield).

^{1}H NMR (500 MHz, CD_2Cl_2) δ 8.22 (d, J = 8.9 Hz, 1H), 5.78 (d, J = 8.9 Hz, 1H), 4.07 – 3.97 (m, 4H), 3.78 – 3.74 (m, 4H),1.50 (s, 6H).

^{13}C NMR (125 MHz, CD_2Cl_2) δ 154.7, 151.5, 149.6, 140.3, 115.3, 105.2, 100.3, 65.7, 48.4, 21.1.

HRMS (m/z, ESI): calcd for $C_{13}H_{17}N_4O_3^+$ [M+H]$^+$: 277.1295, found: 277.1301.

Results and Discussion

Chemical synthesis of a library of C-bridged nitrobenzodiazoles.

Building on the recently reported SCOTfluors,[41] which feature a benzodiazole core as a fluorogenic scaffold, we designed the synthesis of a small collection of C-bridged benzodiazoles using a two-step protocol with a readily accessible common precursor (compound **1**, Figure 2) and commercially available ketone and amine building blocks. We obtained 2-fluoro-4-nitro-*o*-phenylenediamine **1** in good yields and then utilised it in Cu-catalysed condensations with ketones to render the intermediate C-bridged benzodiazoles (**2**, Figure 2). Subsequently, we performed nucleophilic aromatic substitutions to conjugate an array of primary and secondary amines and render the final NIR-emitting products (**3**, Figure 2). First, we employed acetone as the main carbonyl input to enable the formation of the smallest C-bridged benzodiazoles with methyl groups as substituents. In parallel, we also assessed Cu-catalysed condensations with two aromatic ketones (i.e., acetophenone and 4-nitroacetophenone) to explore the scope of the reaction and analyse the effect of different substituents on the spectral properties of C-bridged benzodiazoles. While the condensation of the starting material **1** with acetone proceeded smoothly to afford compound **2a** in 79% yield, acetophenones showed very poor reactivity, likely due to steric hindrance and electron-donating effects. As a result, compounds **2b** and **2c** were isolated only in poor yields (8% and 16%, respectively), even after prolonged heating for multiple days. Attempts at improving these yields by addition of fresh catalyst or additional equivalents of ketone did not improve the poor conversion rates.

Next, the conjugation reactions with a chemically-diverse set of amine building blocks were run in water/acetonitrile in the presence of sodium bicarbonate as a base. These conditions ensured full solubility of the reagents and activation of the nucleophilic amine group. Initially, *N,N'*-diethylamine was employed to assess the reactivity of different benzodiazole intermediates (e.g., compounds **2a**-**2c**). While **2a** underwent a clean conversion into the corresponding **3a** with yields over 80%, derivatives bearing aromatic substituents turned out to be problematic with yields for compounds **3b** and **3c** below 10%. We therefore choose to employ the compound **2a** for further derivatisation and preparation of the C-bridged benzodiazole library. Simple primary amines (e.g., *N*-propylamine, aminohexanoic acid) were found to react well, and both compounds **3d** and **3e** were isolated in moderate yields between 20% and 40%. On the other end, secondary amines other than *N,N'*-diethylamine gave mixed results. Piperidine and *N*-methylallylamine derivatives **3f** and **3g** were also obtained in comparable yields, but the use of *N*-ethylcyclohexylamine rendered compound **3h** in trace amounts. Finally, we also attempted the formation of morpholine and benzylamine derivatives. Of note, during these reactions we observed the formation of double substitution products. For the morpholino derivative we could isolate both mono and disubstituted benzodiazoles (**3i** and **3j**, respectively) whereas the benzylamine derivative was only isolated as the disubstituted analogue (**3k**).

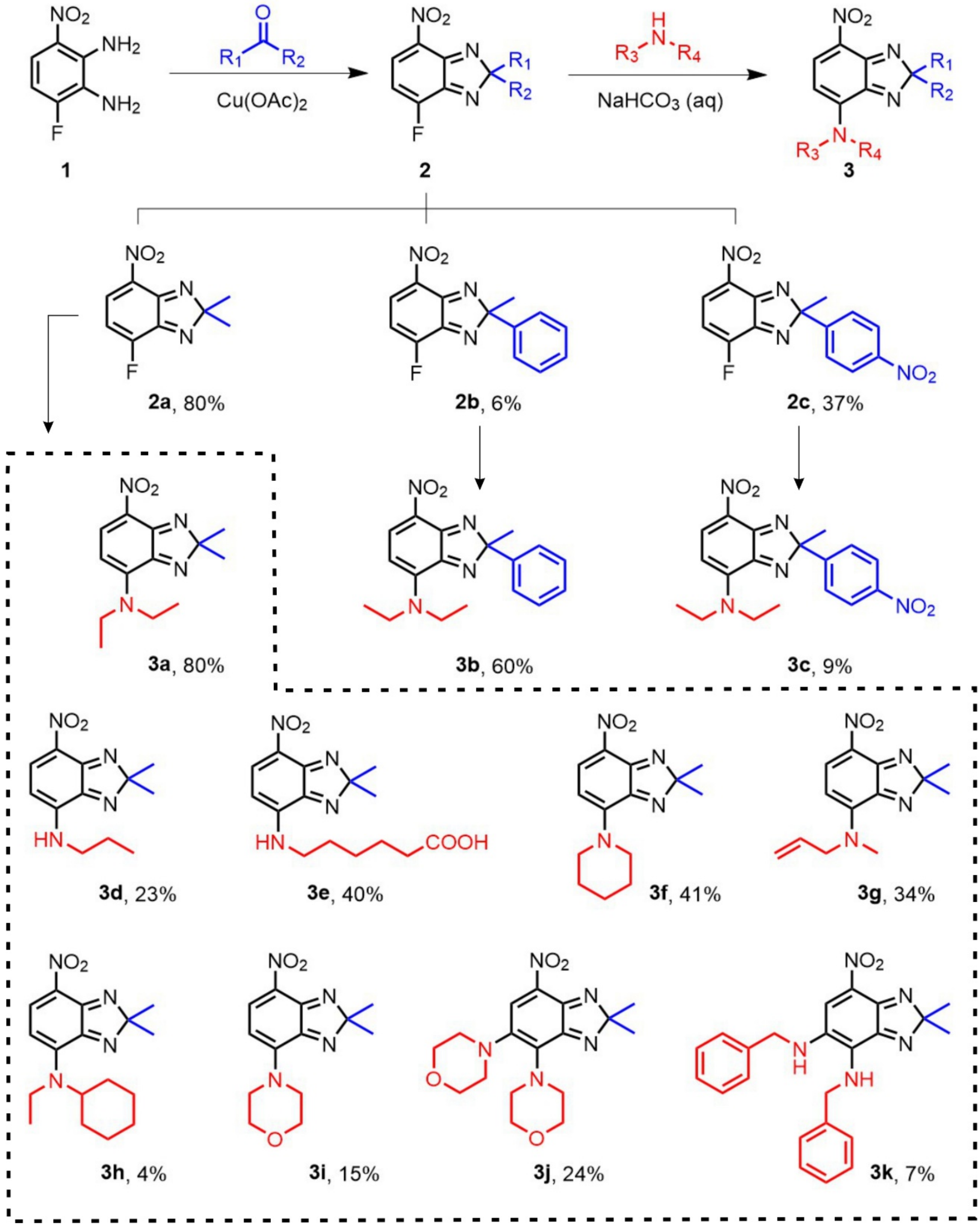

Figure 2. Synthetic strategy for the preparation of NIR-emitting C-bridged benzodiazoles and chemical structures of the isolated compounds with their respective synthetic yields.

In vitro screening of C-bridged nitrobenzodiazoles with biological analytes.

After the synthesis of a collection of C-bridged benzodiazoles, we analysed their spectral properties. Most compounds exhibited absorbance maxima wavelengths around 570 nm and broad fluorescence emission in the 650-750 nm range. Comparative analysis within the library highlighted some differences between the differently substituted compounds **3a**, **3b** and **3c**. Of note, compounds **3b** and **3c**, which incorporate an aromatic residue at the bridging position, displayed around 20 nm longer emission maxima wavelengths than compound **3a**. On the other hand, the incorporation of different amines at the position 4 of the C-bridged benzodiazoles did not lead to major changes in their emission wavelengths (Table S1).

Little is known about the potential of the C-bridged benzodiazole scaffold for the development of fluorescent biomolecules, so we decided to systematically investigate the fluorescence responses of all benzodiazoles against a broad range of biological analytes under physiological conditions. Diversity-oriented fluorescence libraries have proven an effective approach for the identification of environmentally-sensitive fluorophores as well as analyte-responding probes.[42] First, we run a fluorescence response profiling analysis by monitoring the fluorescent intensity changes of 11 C-bridged benzodiazoles against 60 biometabolites including amino acids (asparagine, isoleucine, tyrosine, lysine, tryptophan , alanine, arginine, asparagine, phenylalanine, methionine, proline, valine, glutamine, histidine, leucine, glutamate, serine, glycine and threonine), oxidalnt and reducing agents (cysteine, homocysteine, glutathione, GSSG (glutathione disulfide), H_2O_2, OCl^-, $\cdot OH$, $^1O_2$, NO, NaSH and $\cdot O_2$), sugars (arabinose, glucose, fructose, galactose, sucrose, maltose, mannose and glycogen), steroids (estriol, choric acid, dexamethasone, estrone, β-estradiol, 4-androsterene-3,17-dione), metal ions (Fe^{3+}, Fe^{2+}, Cu^{2+}, Cu^+, Ca^{2+}, Mg^{2+}, Zn^+, Hg^{2+}, Sn^{2+} and Pd^{2+}), nucleic acids (DNA (deoxyribonucleic acid)) and proteins (bovine serum albumin, human serum albumin, lysozyme and peroxidase). To maximise the reliability of our primary screening, we configured the assay conditions with four serial concentrations for each analyte in these ranges: 0.1-100 μM for steroids, 2-2000 μg mL^{-1} for proteins, 0.31-310 pg μL^{-1} for DNA and 1-1000 μM for all other analytes.

A total of 2,640 combinations (11 C-bridged benzodiazoles × 60 analytes × 4 concentrations) were examined. To simplify the visualisation and analysis of the generated data, we calculated the fluorescence intensities for each compound as emission fold changes in the absence and in the presence of the different analytes and plotted them as a pseudo-coloured heat map (Figure 3). The overall average fold change observed for our library of compounds was determined as of 1.098, which indicates that the majority of benzodiazoles remained fluorescently silent and did not show bright emission and highlight their potential as fluorogenic probes. However, some of the screened compounds displayed moderate to good fluorescence increases upon incubation with specific analytes and we could identify several probe/analyte pairs with turn-on responses (for a detailed summary of the screening results, see Table S2). Interestingly, compounds **3i** and **3j**, which both contain morpholine groups, were found to be a notable exception and displayed some remarkable reactivity against metal cations. Compound **3j** showed bright fluorescence emission upon incubation with different metal ions (Fe^{2+}, Cu^{2+}, Cu^{+}, Hg^{2+} and Pd^{2+}) but also displayed high reactivity with other analytes (GSSG, H_2O_2, $\cdot OH$, NO, NaSH and Leu, among others). On the other hand, compound **3i** showed a significant fluorescence emission increase upon 10 min incubation with Fe^{2+} ions in aqueous solution and good selectivity over other metal cations and biologically-relevant molecules (Figure 3). In the view of these results, and due to the biological relevance of iron species and to the ability of this fluorophore to discriminate between very similar analytes (i.e. Fe^{2+} and Fe^{3+} ions), we scaled up the synthesis of compound **3i** for further analytical characterisation.

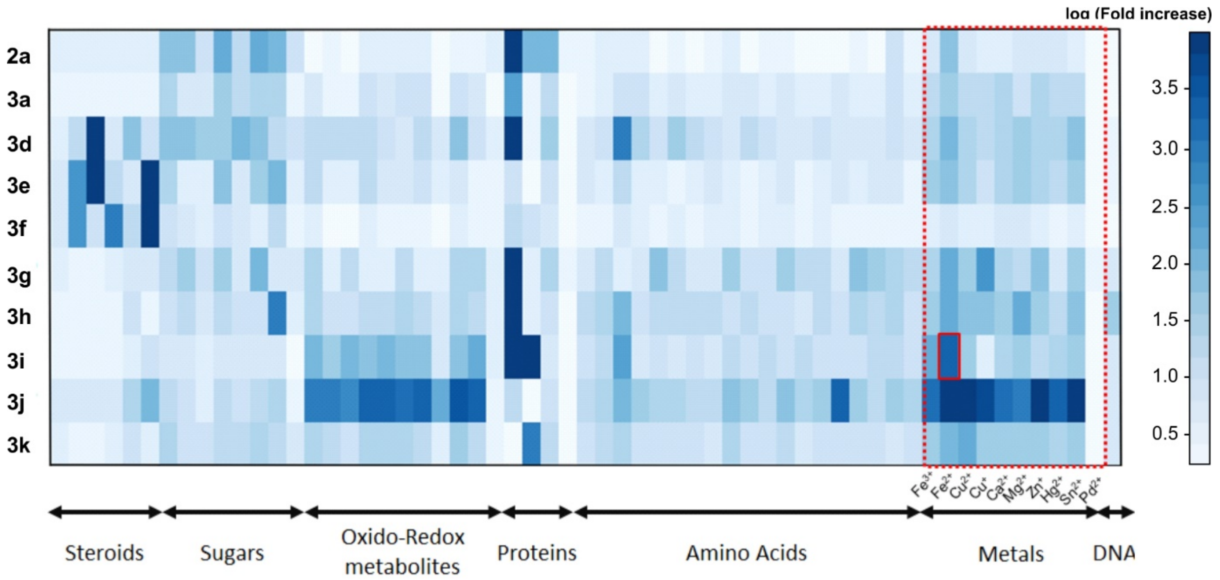

Figure 3. Representative heatmap with the fluorescence intensity of C-bridged benzodiazoles (**2a**-**3k**) at the highest concentration of analyte, including steroids (estriol, choric acid, dexamethasone, estrone, β-estradiol, 4-androsterene-3,17-dione) with 2% EtOH in phosphate buffered saline (PBS) pH 7.4; sugars (arabinose, glucose, fructose, galactose, sucrose, maltose, mannose and glycogen); redox-related molecules (cysteine, homocysteine, glutathione, GSSG (glutathione disulfide), H_2O_2, OCl^-, $\cdot OH$, $^1O_2$, NO, NaSH and $\cdot O_2$); proteins (bovine serum albumin, human serum albumin, lysozyme and peroxidase); amino acids (asparagine, isoleucine, tyrosine, lysine, tryptophan , alanine, arginine, asparagine, phenylalanine, methionine, proline, valine, glutamine, histidine, leucine, glutamate, serine, glycine and threonine); metal ions (Fe^{3+}, Fe^{2+}, Cu^{2+}, Cu^+, Ca^{2+}, Mg^{2+}, Zn^+, Hg^{2+}, Sn^{2+} and Pd^{2+}) and DNA (all of those in PBS pH 7.4). The response of compound **3i** to metal ions is highlighted in red.

Compound 3i shows a differential fluorescence response to Fe^{2+} and Fe^{3+} ions in aqueous media

Iron is an abundant and essential transition metal involved in several physiological processes such as oxygen delivery, electron transport and enzymatic reactions[46]. Disruption of iron homeostasis leads to oxidative stress and cellular damage, which in turn play a significant role in the onset of cardiovascular diseases, neurodegenerative disorders and cancer[47]. Specifically, lysosomes require Fe^{2+} ions to catalyze Fenton-type reactions with hydrogen peroxide to generate reactive oxygen species and contain such species in high micromolar concentrations[48,49].

In order to assess the potential of compound **3i** for the fluorescence detection of Fe^{2+} ions, we first recorded the fluorescence spectra of compound **3i** in aqueous solutions containing different concentrations of the metal cation (Figure 4). Because C-bridged benzodiazoles display low fluorescence quantum yields, concentrations of compound **3i** in the high micromolar range (100-200 μM) were needed to record proper emission spectra. As observed in the primary screening, a slight fluorescence increase was detected in the presence of Fe^{2+} ions (Figure 4a, quantum yield increased from 2.5% to 4.7%). Next, we analysed whether compound **3i** would respond differently to other iron species and observed a clear difference between the fluorescence and colorimetric response to Fe^{2+} and Fe^{3+} solutions at the same concentration, always using chloride as the counteranion. Compound **3i** showed extinction coefficients around 7,800 $M^{-1}cm^{-1}$ at 560 nm (Figure S2) and a clear colorimetric shift from purple to blue from Fe^{2+} to Fe^{3+} together with a drastic reduction of its fluorescence emission (Figure 4b). Notably, we replicated this response when we incubated compound **3i** with solutions of Fe^{2+} that had been treated with ethylenediaminetetraacetic acid (EDTA), which suggests that the behaviour of compound **3i** might be related to the chelation of Fe^{2+} ions. We also performed a Job plot analysis to study the complex formed between compound **3i** and Fe^{2+} and observed a maximal response for a 1:1 stoichiometry (Figure S3). Furthermore, to analyse whether compound **3i** would show a differential aggregation profile in aqueous solutions that contained Fe^{2+} or Fe^{3+} ions, we performed dynamic light scattering experiments. In these assays, we observed the formation of large aggregates when compound **3i** was incubated with aqueous $FeCl_2$ but no changes in aggregation for $FeCl_3$ solutions (Figure 4c).

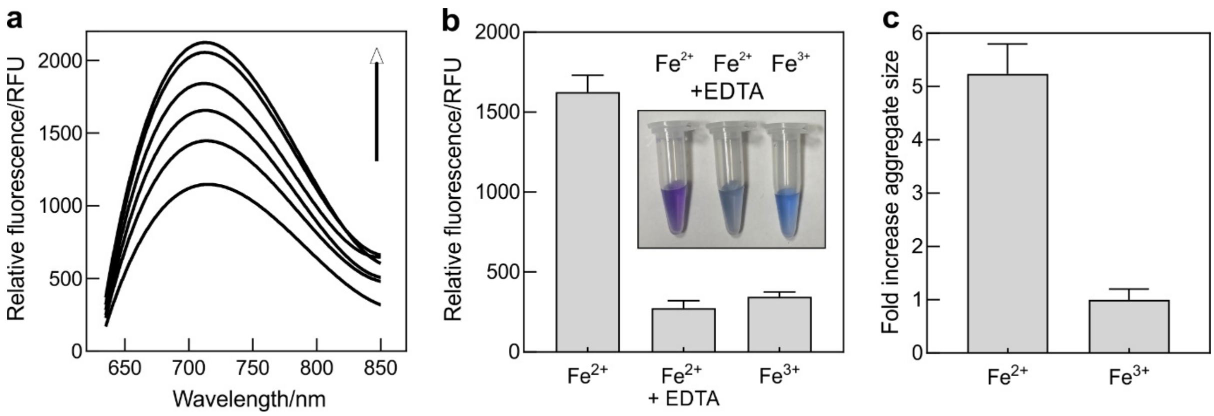

Figure 4. a) Fluorescence spectra of compound **3i** (200 μM) after incubation with increasing concentrations of aqueous $FeCl_2$ (0, 0.125, 0.25, 0.5, 1 and 2 mM), λ_{exc}: 570 nm. b) Fluorescence intensity of compound **3i** (200 μM) after incubation with different iron species ($FeCl_2$ and $FeCl_3$: 1 mM; EDTA: 1 mM). Inset) Pictograms of the different solutions under white

light. c) Dynamic light scattering measurement of aggregates formed after 60-min incubation of compound **3i** (200 μM) with 2 mM $FeCl_2$ or 2 mM $FeCl_3$. Plots shows the relative increase aggregate size when compared to an aqueous solution of compound **3i** (200 μM). Data presented as means ± SD (n=3-6).

Altogether, our results indicate compound **3i** as a fluorogenic molecule for the detection of Fe^{2+} in aqueous media with a clear differential response to other metal cations, particularly to Fe^{3+} ions. Future studies with compound **3i** will involve its evaluation as a probe for imaging the trafficking of intracellular Fe^{2+} in live cells.

Conclusions

In summary, herein we report the synthesis of the first small collection of C-bridged benzodiazoles and their systematic characterisation as potential fluorogenic molecules with NIR emission. Through a diversity-oriented fluorescence screening using 60 chemically-diverse biomolecules, we observed that C-bridged benzodiazoles are inherently silent molecules and with potential to turn on their fluorescence response upon incubation with different analytes. From our screening we observed that morpholino-containing benzodiazoles showed remarkable response against metal cations and we further studied the behaviour of compound **3i** for the detection of Fe^{2+} ions. Compound **3i** showed increased fluorescence emission in the presence of equal amounts of Fe^{2+} ions, whereas the signals were drastically reduced in the presence of Fe^{3+} ions. Mechanistic assays suggest that the response of compound **3i** might be related to chelation -as seen in experiments with EDTA- or aggregation -followed by light scattering experiments-. The expansion of the C-bridged benzodiazole toolbox with additional commercially-available amine and/or ketone building blocks will accelerate the development of NIR chemosensors with multiple applications in analytical and biological chemistry.

Author information

Corresponding authors: junseoklee@korea.ac.kr, marc.vendrell@ed.ac.uk.

Notes

The authors declare no conflicts of interest.

Acknowledgments

The authors acknowledge funding from Medical Research Scotland (S.B.: 879-2015) and an ERC Consolidator Grant (DYNAFLUORS, M. V.: 771443). This work was also supported by National Research Foundation funded by the Ministry of Science, ICT & Future Planning, South Korea (J. S. L.: NRF-2018M3A9H4079286, NRF-2020R1A2C2004422).

References

1. Park S J, Yeo H C, Kang N Y, Kim H, Lin J, Ha H H, Vendrell M, Lee J S, Chandran Y, Lee D Y, et al. Mechanistic elements and critical factors of cellular reprogramming revealed by stepwise global gene expression analyses. Stem Cell Research, 2014, 12(3): 730–741.

2. Carter K P, Young A M, Palmer A E. Fluorescent sensors for measuring metal ions in living systems. Chemical Reviews, 2014, 114(8): 4564–4601.

3. Jiao X Y, Li Y, Niu J Y, Xie X L, Wang X, Tang B. Small-molecule fluorescent probes for imaging and detection of reactive oxygen, nitrogen, and sulfur species in biological systems. Analitycal Chemistry, 2018, 90(1): 533–555.

4. Han J Y, Burgess K. Fluorescent indicators for intracellular pH. Chemical Reviews, 2010, 110(5): 2709–2728.

5. Dedecker P, De Schryver F C, Hofkens J. Fluorescent Proteins: Shine on, you crazy diamond. Journal of the American Chemical Society, 2013, 135(7): 2387–2402.

6. Gong J, Liu C, Jiao X J, He S, Zhao L C, Zeng X S. A novel near-infrared fluorescent probe with an improved Stokes shift for specific detection of Hg^{2+} in mitochondria. Organic and Biomolecular Chemistry, 2020, 18(27): 5238–5244.

7. Kwon H Y, Liu X, Choi E G, Lee J Y, Choi S Y, Kim J Y, Wang L, Park S J, Kim B, Lee Y A, et al. Development of a universal fluorescent probe for gram-positive bacteria. Angewandte Chemie International Edition, 2019, 58(25): 8426–8431.

8. Devaraj N K, Weissleder R. Biomedical applications of tetrazine cycloadditions. Accounts of Chemical Research, 2011, 44(9): 816–827.

9. Chen G Q, Guo Z, Zeng G M, Tang L. Fluorescent and colorimetric sensors for environmental mercury detection. Analyst, 2015, 140(16): 5400–5443.

10. Chan J, Dodani S C, Chang C J. Reaction-based small-molecule fluorescent probes for chemoselective bioimaging. Nature Chemistry, 2012, 4(12): 973–984.

11. Duong T Q, Kim J S. Fluoro- and chromogenic chemodosimeters for heavy metal ion detection in solution and biospecimens. Chemical Reviews, 2010, 110(10): 6280–6301.

12. Yraola F, Ventura R, Vendrell M, Colombo A, Fernandez J C, de la Figuera N, Fernandez-Forner D, Royo M, Forns P, Albericio F. A re-evaluation of the use of rink, BAL, and PAL resins and linkers. Qsar Combinatorial Science, 2004, 23(2-3): 145–152.
13. Sainlos M, Iskenderian W S, Imperiali B. A general screening strategy for peptide-based fluorogenic ligands: probes for dynamic studies of PDZ domain-mediated interactions. Journal of the American Chemical Society, 2009, 131(19): 6680–6682.
14. Kalstrup T, Blunck R. Dynamics of internal pore opening in K(V) channels probed by a fluorescent unnatural amino acid. Proceedings of the National Academy of Sciences of the United States of America, 2013, 110(20): 8272–8277.
15. Sachdeva A, Wang K H, Elliott T, Chin J W. Concerted, rapid, quantitative, and site-specific dual labeling of proteins. Journal of the American Chemical Society, 2014,136(22): 7785 –7788.
16. Lampkowski J S, Uthappa, D M, Young D D. Site-specific incorporation of a fluorescent terphenyl unnatural amino acid. Bioorganic and Medicinal Chemistry Letters, 2015, 25(22), 5277–5280.
17. FitzGerald L I, Aurelio L, Chen M, Yuen D, Rennick J J, Graham B, Johnston A P R. A molecular sensor to quantify the localization of proteins, DNA and nanoparticles in cells. Nature Communications, 2020, 11(1): 1–13.
18. Fernandez A, Vermeren M, Humphries D, Subiros-Funosas R, Barth N, Campana L, MacKinnon A, Feng Y, Vendrell M. Chemical modulation of in vivo macrophage function with subpopulation-specific fluorescent prodrug conjugates. ACS Central Science, 2017, 3(9): 995–1005.
19. Subiros-Funosas R, Mendive-Tapia L, Sot J, Pound J D, Barth N, Varela Y, Goni F M, Paterson M, Gregory C D, Albericio F, et al. A Trp-BODIPY cyclic peptide for fluorescence labelling of apoptotic bodies. Chemical Communications, 2017, 53(5): 945–948.
20. Barth N D, Subiros-Funosas R, Mendive-Tapia L, Duffin R, Shields M A, Cartwright J A, Henriques S T, Sot J, Goni F M, Lavilla R, et al. A fluorogenic cyclic peptide for imaging and quantification of drug-induced apoptosis. Nature Communications, 2020, 11(1): 1–14.

21. Osseiran S, Austin L A, Cannon T M, Yan C, Langenau D M, Evans C L. Longitudinal monitoring of cancer cell subpopulations in monolayers, 3D spheroids, and xenografts using the photoconvertible dye DiR. Scientific Reports, 2019, 9: 1–10.

22. Anorma C, Hedhli J, Bearrood T E, Pino N W, Gardner S H, Inaba H, Zhang P, Li Y F, Feng D, Dibrell S E, et al. Surveillance of cancer stem cell plasticity using an isoform-selective fluorescent probe for aldehyde dehydrogenase 1A1. ACS Central Science, 2018, 4(8): 1045–1055.

23. Barth N D, Marwick J A, Vendrell M, Rossi A G, Dransfield I. The "Phagocytic synapse" and clearance of apoptotic cells. Frontiers in Immunology, 2017, 8: 1708–1717.

24. Yi Z, Luo Z, Barth N D, Meng X, Liu H, Bu W, All A, Vendrell M, Liu, X. In vivo tumor visualization through MRI off-on switching of NaGdF4-CaCO3 nanoconjugates. Advanced Materials, 2019, 31(37): e1901851.

25. Samanta A, Vendrell M, Yun S W, Guan Z, Xu Q H, Chang Y T. A photostable near-infrared protein labeling dye for in vivo imaging. Chemistry: An Asian Journal, 2011, 6(6): 1353–1357.

26. Chen C, Tian R, Zeng Y, Chu C C, Liu G. Activatable fluorescence probes for "turn-on" and ratiometric biosensing and bioimaging: from NIR-I to NIR-II. Bioconjugate Chemistry, 2020, 31(2): 276–292.

27. Wang P Y, Fan Y, Lu L F, Liu L, Fan L L, Zhao M Y, Xie Y, Xu C J, Zhang F. NIR-II nanoprobes in-vivo assembly to improve image-guided surgery for metastatic ovarian cancer. Nature Communications, 2018, 9: 1–10.

28. Vahrmeijer A L, Hutteman M, van der Vorst J R. van de Velde C J H, Frangioni J V. Image-guided cancer surgery using near-infrared fluorescence. Nature Reviews Clinical Oncology, 2013, 10(9): 507–518.

29. Guo Z Q, Park S, Yoon J, Shin I. Recent progress in the development of near-infrared fluorescent probes for bioimaging applications. Chemical Society Reviews, 2014, 43(1): 16–29.

30. Wirth R, Gao P, Nienhaus G U, Sunbul M, Jaschke A. SiRA: a silicon rhodamine-binding aptamer for live-cell super-resolution RNA imaging. Journal of the American Chemical Society, 2019, 141(18): 7562–7571.

31. Koide Y, Urano Y, Hanaoka K, Piao W, Kusakabe M, Saito N, Terai T, Okabe T, Nagano T. Development of NIR fluorescent dyes based on Si-rhodamine for in vivo imaging. Journal of the American Chemical Society, 2012, 134(11): 5029–5031.

32. Ramos A A, Nascimento F B, de Souza T F M, Omori A T, Manieri T M, Cerchiaro G, Ribeiro A O. Photochemical and photophysical properties of phthalocyanines modified with optically active alcohols. Molecules, 2015, 20(8): 13575–13590.

33. Pal A K, Varghese S, Cordes D B, Slawin A M Z, Samuel I D W, Zysman-Colman E. Near-infrared fluorescence of silicon phthalocyanine carboxylate esters. Scientific Reports, 2017, 7, 1–14.

34. Wong R C H, Lo P C, Ng D K P. Stimuli responsive phthalocyanine-based fluorescent probes and photosensitizers. Coordination Chemistry Review 2019, 379: 30–46.

35. Ilina K, MacCuaig W M, Laramie M, Jeouty J N, McNally L R, Henary M. Squaraine dyes: molecular design for different applications and remaining challenges. Bioconjugate Chemistry, 2020, 31(2): 194–213.

36. Xia G M, Wang H M. Squaraine dyes: The hierarchical synthesis and its application in optical detection. Journal of Photochemistry and Photobiology C, 2017, 31: 84–113.

37. Mathew S, Yella A, Gao P, Humphry-Baker R, Curchod B F E, Ashari-Astani N, Tavernelli I, Rothlisberger U, Nazeeruddin M K, Gratzel M. Dye-sensitized solar cells with 13% efficiency achieved through the molecular engineering of porphyrin sensitizers. Nature Chemistry 2014, 6(3): 242–247.

38. Mellanby R J, Scott J I, Mair I, Fernandez A, Saul L, Arlt J, Moral M, Vendrell M. Tricarbocyanine N-triazoles: the scaffold-of-choice for long-term near-infrared imaging of immune cells in vivo. Chemical Science 2018, 9(36): 7261–7270.

39. Okuda K, Okabe Y, Kadonosono T, Ueno T, Youssif B G M, Kizaka-Kondoh S, Nagasawa H. 2-Nitroimidazole-tricarbocyanine conjugate as a near-infrared fluorescent probe for in vivo imaging of tumor hypoxia. Bioconjugate Chemistry, 2012, 23(3): 324–329.
40. Cosco E D, Caram J R, Bruns O T, Franke D, Day R A, Farr E P, Bawendi M G, Sletten E M. Flavylium polymethine fluorophores for near- and shortwave infrared imaging. Angewandte Chemie International Edition, 2017, 56(42): 13126–13129.
41. Benson S, Fernandez A, Barth N D, de Moliner F, Horrocks M H, Herrington C S, Abad J L, Delgado A, Kelly L, Chang Z, et al. SCOTfluors: small, conjugatable, orthogonal, and tunable fluorophores for In vivo imaging of cell metabolism. Angewandte Chemie International Edition, 2019, 58(21): 6911–6915.
42. Yun S W, Kang N Y, Park S J, Ha H H, Kim Y K, Lee J S, Chang Y T. Diversity oriented fluorescence library approach (DOFLA) for live cell imaging probe development. Accounts of Chemical Research, 2014, 47(4): 1277–1286.
43. Lee J S, Vendrell M, Chang Y T. Diversity-oriented optical imaging probe development. Current Opinion in Chemical Biology, 2011, 15(6): 760–767.
44. Luo X, Qian L J, Xiao Y S, Tang Y, Zhao Y, Wang X, Gu L Y, Lei Z H, Bao J M, Wu J H, et al. A diversity-oriented rhodamine library for wide-spectrum bactericidal agents with low inducible resistance against resistant pathogens. Nature Communications, 2019, 10: 1–12.
45. Burchak O N, Mugherli L, Ostuni M, Lacapere J J, Balakirev M Y. Combinatorial discovery of fluorescent pharmacophores by multicomponent reactions in droplet arrays. Journal of the American Chemical Society, 2011, 133(26): 10058–10061.
46. Kaplan J, Ward D M. The essential nature of iron usage and regulation. Current Biology, 2013, 23(15): R642–R646.
47. Dev S, Babitt J L. Overview of iron metabolism in health and disease. Hemodialysis International, 2017, 21: S6–S20.
48. Trivedi P C, Bartlett J J, Pulinilkunnil T. Lysosomal Biology and Function: Modern view of cellular debris bin. Cells, 2020, 9(5): 1131–1166.
49. Xu H, Ren D. Lysosomal physiology. Annual Review of Physiology 2015, 77: 57–80.